

# Superluminal waves in pulsar winds

Ioanna Arka<sup>1</sup> and John G. Kirk

Max-Planck-Institut für Kernphysik, Postfach 10 39 80, 69029 Heidelberg, Germany

`ioanna.arka@mpi-hd.mpg.de`, `john.kirk@mpi-hd.mpg.de`

Received \_\_\_\_\_; accepted \_\_\_\_\_

## ABSTRACT

The energy lost by a rotation-powered pulsar is carried by a relativistic flow containing a mixture of electromagnetic fields and particles. In the inner regions, this is thought to be a magnetically dominated, cold, electron-positron wind that is well described by the MHD equations. However, beyond a critical radius  $r_{\text{cr}}$ , the same particle, energy and momentum fluxes can be transported by a strong, transverse electromagnetic wave with superluminal phase speed. We analyze the nonlinear dispersion relation of these waves for linear and circular polarization, and find the dependence of  $r_{\text{cr}}$  on the mass-loading, magnetization and luminosity of the flow, as well as on the net magnetic flux. We show that, for most isolated pulsars, the wind lies well outside  $r_{\text{cr}}$ , and speculate that superluminal modes play an important role in the dissipation of electromagnetic energy into nonthermal particles at the termination shock.

*Subject headings:* plasmas – waves – acceleration of particles – pulsars:general – stars: winds, outflows

## 1. Introduction

Pulsar winds are believed to be launched as relativistic outflows consisting mainly of electrons and positrons. These winds are Poynting-flux dominated when they are launched from the pulsar. Outside the light-cylinder (located at  $\rho = r/r_{\text{LC}} = r\Omega/c = 1$ , with  $\Omega$  the angular velocity of the pulsar) they move radially, carrying a frozen-in, nearly transverse magnetic field that is modulated by the pulsar rotation. They can be viewed as nonlinear waves, whose phase speed equals the radial flow speed (and is, therefore, subluminal). The simplest analytic description of this flow is the “striped wind” (Coroniti 1990), in which the magnetic field is purely toroidal, has a magnitude proportional to  $1/r$ , and reverses sign across a corrugated current sheet that separates the two magnetic hemispheres. Numerical solutions of the force-free, oblique rotator problem (Spitkovsky 2006), lend qualitative support to this picture, which has also been used to model the high-energy emission of pulsars (Pétri & Kirk 2005; Pétri 2011) as well as the orbital modulation of the high and very high energy emission from gamma-ray binaries that contain pulsars (Pétri & Dubus 2011).

In the absence of dissipation, these subluminal waves propagate at constant speed and remain Poynting dominated, provided their density is high enough to apply the MHD approximation (Kirk & Mochol 2011a). However, basic dynamical considerations indicate that the winds should not be Poynting dominated after they cross the termination shock (Rees & Gunn 1974; Begelman 1998), and spectral and morphological modeling of pulsar wind nebulae suggest an even stricter upper limit on the Poynting dominance. How Poynting flux is converted to kinetic energy flux is still not clear (for reviews see Gaensler & Slane 2006; Kirk et al. 2009). Reconnection in the current sheet, as proposed

---

<sup>1</sup>present address: Institute de Planétologie et d’Astrophysique de Grenoble, UMR 5274, BP 53 F-38041 Grenoble, France

by Coroniti (1990) and Michel (1994), proceeds rather slowly (Lyubarsky & Kirk 2001; Kirk & Skjæraasen 2003; Lyubarsky 2010). In the case of an isolated pulsar such as the Crab, it fails to convert a significant fraction of the electromagnetic flux before the flow reaches the termination shock, unless the rate of pair injection by the pulsar is much higher than conventionally assumed (Arons 2011).

Motivated by this finding, Lyubarsky (2003) suggested that the fields are dissipated in the termination shock itself. This is not permitted at an MHD shock in a strongly magnetized flow, where the compression ratio remains close to unity. Nevertheless, it is possible to imagine a viable scenario in which reconnection in the current sheet of a striped wind is driven or triggered by the relatively weak compression of the MHD shock (Pétri & Lyubarsky 2007; Lyubarsky & Liverts 2008). Recent 2D and 3D PIC simulations exhibit such an effect (Sironi & Spitkovsky 2011), albeit at even higher pair injection rates than those suggested by Arons (2011).

An alternative picture is offered by superluminal waves. Because the density in the wind falls with increasing radius, these modes, which are absent in the MHD description, can propagate outside of a certain critical radius  $r_{\text{cr}}$  (Usov 1975; Melatos & Melrose 1996). If this radius lies inside the termination shock, the possibility arises that the flow converts from a subluminal to a superluminal wave either spontaneously at some point upstream of the shock, or as an integral part of the shock itself. The latter possibility is an attractive scenario, since these modes are known to damp much more rapidly than the subluminal striped wind mode (Lee & Lerche 1978; Asseo et al. 1980), guaranteeing a relatively thin transition region.

At low amplitudes, transverse, superluminal waves in an electron-positron plasma have simple properties (e.g., Iwamoto 1993). However, under pulsar conditions, the waves are strongly nonlinear. Their properties have been investigated in many papers, (for

example Kaw & Dawson 1970; Max & Perkins 1971; Clemmow 1974, 1977; Asseo et al. 1984; Melatos & Melrose 1996; Skjæraasen et al. 2005). Here we take a new look at the problem, and extend the known results for both circularly polarized waves, and linearly polarized waves with a non-zero (phase-averaged) magnetic field, using the two-fluid (electron-positron) model. In particular, we formulate and solve the equations that determine into which modes a striped wind of given magnetization can convert. This amounts to solving the electrodynamic equivalent of the jump conditions across a magnetohydrodynamic shock front. As a result, we find the cut-off radius of these modes as a function of the striped wind parameters. We also show that the frequently used “strong wave limit” does not provide an adequate description of these modes.

The paper is set out as follows: in Section 2 we review the basic equations for plane waves. Using the “homogeneous” or “H-frame” formulation introduced by Clemmow (1974, 1977), we compute the fluxes of particles, energy and momentum carried as functions of the wave parameters. In Section 3, we use these relations to solve the jump conditions that must be fulfilled when the wind converts from a subluminal to a superluminal mode across a transition layer that is narrow compared to its distance from the pulsar. Section 4 contains a discussion of these results and their relation to the problem of dissipation at the termination shock.

## 2. Superluminal waves in an electron-positron plasma

An analytical treatment of non-linear waves in a cold plasma was first undertaken by Akhiezer & Polovin (1956) who considered a one-component electron plasma in a background of fixed ions. In their approach, all wave quantities depend only on the phase  $\phi$  of the wave. For waves propagating in the  $x$ -direction,  $\phi = \omega(t - x/v_\phi)$ , where  $v_\phi$  is the phase velocity and  $\omega$  the frequency of the wave. Both subluminal and superluminal waves

( $v_\phi < c$  and  $v_\phi > c$  respectively) are possible, and the longitudinal and transverse modes are, in general, coupled. Pulsars are most likely surrounded by an electron-positron pair plasma, possibly loaded with a small number of protons, so that a single-fluid approximation is not valid. Also, the wave amplitudes near the pulsar are expected to be high enough to drive even the proton component of a plasma to relativistic velocity, suggesting that the rest mass of the fluid particles is unimportant. Consequently, rather than considering the general case of an electron-ion plasma, attention has been concentrated on the much simpler two-fluid electron-positron plasma. In such a plasma, both linearly and circularly polarized waves with purely transverse fields can propagate without introducing fluctuations in the charge-density (Asseo et al. 1975; Kennel & Pellat 1976). It is these waves that we consider in the following.

Far from the pulsar (at  $\rho \gg 1$ ), the magnetic field is twisted into a tightly-wound spiral form, and it is an excellent approximation to neglect the phase-averaged radial field component compared to the toroidal one. Since pulsar winds are radial, this means that the phase-averaged component of the magnetic field is transverse. Furthermore, in this region, the radius of curvature of the wavefront is much larger than one wavelength, so that the waves can be approximated as locally plane.

In the following, we identify the (radial) propagation direction of the wave as the  $x$ -axis and the toroidal direction as the  $z$ -axis, so that  $E_x = 0$  and  $B_x = 0$ . The equations to be solved are the continuity equations and the equations of motion for each of the two particle species, along with Maxwell's equations. These are given in Appendix A, where it is shown that, from Maxwell's equations and making use of the assumption of purely transverse waves, the two species have the same density:  $\gamma_+ n_+ = \gamma_- n_-$  (a plus (minus) subscript denotes positrons (electrons)). Furthermore, the Lorentz factors are equal:  $\gamma_+ = \gamma_-$  and

the other components of the dimensionless four-velocity of the two species are related by:

$$u_{x+} = u_{x-} \quad u_{y+} = -u_{y-} \quad u_{z+} = -u_{z-} .$$

To keep the notation simple, we henceforth drop the plus and minus subscripts and express everything in terms of the positron fluid quantities.

For superluminal waves, Clemmow (1974, 1977) showed the problem is significantly simplified if one performs the calculations in a frame of reference that propagates with a speed  $c^2/v_\phi$  with respect to the lab. frame. In this frame, which we call the H-frame, the wave quantities do not depend on space but only on time, and the phase of the wave is just  $\phi = \omega t$ . An immediate consequence of Faraday's equation is that in this frame the magnetic field, in addition to being homogeneous, is also constant. In the following, unprimed symbols denote quantities in the H-frame; we use primed symbols for quantities in the lab. frame.

## 2.1. Circular polarization

The circularly polarized wave is described in the H-frame by three (phase-independent) parameters: the (constant) proper number density of each species  $n = n_0$ , the component of the four-velocity in the direction of propagation  $u_x = u_{x0}$ , and the magnitude of the four-velocity component perpendicular to the propagation direction  $\sqrt{u_y^2 + u_z^2}$ , which, for this wave mode, equals the dimensionless *strength parameter* denoted by  $a$  and defined in terms of the electric field amplitude  $E_0$  as

$$a = e |E_0| / (mc\omega) . \tag{1}$$

Consequently, the Lorentz factor of the fluids is also phase-independent:  $\gamma = \gamma_0 = \sqrt{1 + u_{x0}^2 + a^2}$ . The frequency  $\omega$  coincides with the (proper) plasma frequency,  $\omega_p$ :

$$\omega = \omega_p = \sqrt{\frac{8\pi n_0 e^2}{m}} . \tag{2}$$

In terms of these quantities, the particle flux density  $J$  and the  $(0, 0)$ ,  $(0, x)$  and  $(x, x)$  components of the stress energy tensor are given by (see Appendix B, equations A37-A39 and A40-A42):

$$J = n_0 \gamma_0 c \left( \frac{2u_{x0}}{\gamma_0} \right) \quad (3)$$

$$T^{00} = n_0 \gamma_0 m c^2 \left( 2\gamma_0 + \frac{a^2}{\gamma_0} \right) \quad (4)$$

$$T^{01} = n_0 \gamma_0 m c^2 (2u_{x0}) \quad (5)$$

$$T^{11} = n_0 \gamma_0 m c^2 \left( \frac{2u_{x0}^2}{\gamma_0} + \frac{a^2}{\gamma_0} \right) \quad (6)$$

and are also phase-independent.

## 2.2. Linear polarization

The linearly polarized mode requires an additional parameter to fix the amplitude of the phase-averaged magnetic field. In the H-frame, the four parameters are: the proper number density  $n_0$  and the component  $u_{x0}$  of the four velocity in the direction of propagation *both taken at phase zero*, (the point in the wave where the magnitude of the electric field is maximal, and  $u_z = u_y = 0$ ), the nonlinearity parameter  $q$ , used by Kennel & Pellat (1976), and the ratio  $\lambda$  of the (phase-independent) magnetic field to the electric field  $E_0$  at phase zero. Physically  $q$  is double the ratio at phase zero of the energy density in the fluids to that in the electric field, as measured in the H-frame:

$$q = \frac{32\pi n_0 \gamma_0^2 m c^2}{E_0^2} . \quad (7)$$



Defining the normalized field variable  $y = E/E_0$ , one finds:

$$u_x = u_{x0} + 4\gamma_0(1 - y)\lambda/q \quad (8)$$

$$\gamma = \gamma_0 + 2\gamma_0(1 - y^2)/q \quad (9)$$

$$u_y = 0 \quad (10)$$

$$\begin{aligned} |u_z| &= \sqrt{\gamma^2 - u_x^2 - 1} \\ &= 2\gamma_0\sqrt{N(y)}/q \end{aligned} \quad (11)$$

where  $N(y)$  is a fourth-order polynomial, as follows from (8) and (9), and  $\gamma_0 = \sqrt{1 + u_{x0}^2}$ . Periodic wave solutions exist provided  $N(y)$  has four distinct real roots  $y_{1..4}$ , in which case  $y$  oscillates between the values  $y_2$  and  $y_3$  (assuming the ordering  $y_1 < y_2 < y_3 < y_4$ ). Because of the normalization of  $y$ , one has  $y_3 = 1$  and  $|y_2| \leq 1$ . The strength parameter of the wave, as defined in (1) is

$$a = \frac{2}{\pi} \int_{y_2}^1 dy \gamma / \sqrt{N(y)} \quad (12)$$

and the wave frequency is given by

$$\omega = \frac{2\gamma_0}{a\sqrt{q}}\omega_p . \quad (13)$$

The phase-averaged fluxes are:

$$\langle J \rangle = n_0\gamma_0c \left\langle \frac{2u_x}{\gamma} \right\rangle \quad (14)$$

$$\langle T^{00} \rangle = n_0\gamma_0mc^2 \left\langle 2\gamma + \frac{4\gamma_0(y^2 + \lambda^2)}{q} \right\rangle \quad (15)$$

$$\langle T^{01} \rangle = n_0\gamma_0mc^2 \left\langle 2u_x + \frac{8\gamma_0y\lambda}{q} \right\rangle \quad (16)$$

$$\langle T^{11} \rangle = n_0\gamma_0mc^2 \left\langle \frac{2u_x^2}{\gamma} + \frac{4\gamma_0(y^2 + \lambda^2)}{q} \right\rangle \quad (17)$$

and the phase-averaged electric field is

$$\frac{\langle E \rangle^2}{4\pi} = n_0\gamma_0mc^2 \left( \frac{4\gamma_0 \langle y \rangle^2}{q} \right) . \quad (18)$$

Ampère’s law enables these averages to be expressed as integrals over the normalized electric field  $y$ :

$$\langle A(y) \rangle = \frac{\int_{y_2}^1 dy A(y) \gamma / \sqrt{N(y)}}{\int_{y_2}^1 dy \gamma / \sqrt{N(y)}} \quad (19)$$

(see Appendix A).

If the phase-averaged magnetic field vanishes ( $\lambda = 0$ ) one finds  $y_2 = -1$ , and the integrals in (13)–(18) can be expressed in closed form in terms of elliptic integrals. For  $\lambda \neq 0$ , closed forms can be found to lowest order in an expansion in the small parameter  $q$  (see Kennel & Pellat 1976). However, these are not adequate to describe the pulsar case, as we show in the following section. In the general case, one must resort to numerical integration, noting that the integrands have integrable singularities at each of the limits.

### 2.3. Conserved quantities

In order to identify those parts of the wind of a given pulsar in which superluminal waves can propagate, one has to associate the wave properties with wind quantities inferred from the observational data. A pulsar wind transports particles, energy and magnetic flux, and exerts a ram-pressure on its surroundings. Across a stationary shock front the quantities  $J'$ ,  $T'^{01}$  and  $T'^{11}$  are conserved. Also, from Faraday’s law, the transverse electric field component  $E'$  is conserved. Across a thin transition front where one wave-mode converts into another, and which is stationary on the oscillation timescale, the *phase-averaged* values of these quantities are conserved.

However, it is the relative magnitudes of these quantities, rather than their absolute values, that determine the physics of wave propagation. We therefore introduce three

dimensionless quantities:

$$\mu = \frac{\langle T'^{01} \rangle}{mc \langle J' \rangle} \quad (20)$$

$$\nu = \frac{\langle T'^{11} \rangle}{mc \langle J' \rangle} \quad (21)$$

$$\eta = \frac{\langle E' \rangle^2 / 4\pi}{mc \langle J' \rangle} \quad (22)$$

which are conserved across a transition layer and are independent of the density parameter  $n_0$ .  $\mu$  is the mass-loading parameter introduced by Michel (1969), which corresponds to the Lorentz factor each particle would need if they were to carry the entire energy flux.

For the superluminal wave modes discussed above, these quantities can be computed by Lorentz transforming their values in the H-frame into the pulsar, or lab. frame. A boost of (dimensionless) speed  $\beta_{>} = c/v_\phi$  in the negative  $x$  direction is required, for which explicit expressions are given in Appendix B. (We use the notation  $\beta_{>}$  and  $\Gamma_{>}$  for the speed and associated Lorentz factor of the H-frame of the superluminal wave, and  $\beta_{<}$  and  $\Gamma_{<}$  for the phase (or bulk) speed and associated Lorentz factor of the subluminal wave, both as seen from the lab. (pulsar) frame.) Applying these boosts, one obtains, for linearly polarized modes, expressions for  $\mu$ ,  $\nu$  and  $\eta$ , as functions of the four input parameters  $u_{x0}$ ,  $q$ ,  $\lambda$  and  $\beta_{>}$  that must be evaluated by numerical integration. The case of circular polarization, where  $\eta = 0$ , is much simpler, since  $\mu$  and  $\nu$  are given in closed form as functions of  $u_{x0}$ ,  $a$  and  $\beta_{>}$ .

For the cold subluminal wave modes, such as the striped wind (in the absence of dissipation),  $\mu$  and  $\nu$  are independent of radius in the inner parts of the wind where a single-fluid MHD description is adequate (Kirk & Mochol 2011a). Their values can be estimated from standard pulsar models (e.g., Lyubarsky & Kirk 2001). However, these two quantities are almost equal in highly relativistic winds, and it proves more convenient to use, instead of  $\nu$ , the magnetization parameter  $\sigma$ , defined as the ratio of magnetic to

particle energy flux according to:

$$\mu = \Gamma_{<}(1 + \sigma) \quad (23)$$

$$\nu = \frac{\Gamma_{<}^2(1 + \sigma) - (1 + \sigma/2)}{\sqrt{\Gamma_{<}^2 - 1}} \quad (24)$$

In the striped wind, the third parameter,  $\eta$ , depends on the phase-averaged magnetic field value

$$b = \langle B' \rangle / \langle B'^2 \rangle^{1/2} , \quad (25)$$

via the expression:

$$\eta = b^2 \sigma \beta_{<} \Gamma_{<} . \quad (26)$$

Without loss of generality, we may choose  $\langle B' \rangle \geq 0$ , so that  $0 \leq b \leq 1$ . Both  $b$  and  $\eta$  are functions of latitude in the striped pulsar wind, since the spacing in phase of the current sheets varies. At latitudes greater than the inclination angle between the magnetic and rotation axes, conventionally denoted by  $\alpha$ , the sheets vanish (zero spacing), whereas on the equator, they are equally spaced (separated in phase by  $\pi$ ).

Thus, for given  $\mu$ ,  $\sigma$  and  $b$ , the jump conditions can be solved for three of the four input parameters  $u_{x0}$ ,  $q$ ,  $b$  and  $\beta_{>}$ , provided the fourth is specified. The wave frequency, normalized to  $\omega_p$ , can then be constructed from (13).

### 3. Results

#### 3.1. Circular polarization

For circular polarization, the jump conditions can be solved analytically (Kirk 2010). An example is plotted in Fig. 1, which shows the refractive index  $ck'/\omega' = \beta_{>}$ , the strength parameter  $a$  and the component of the particle speed in the propagation direction,  $u_{x0}$ , as

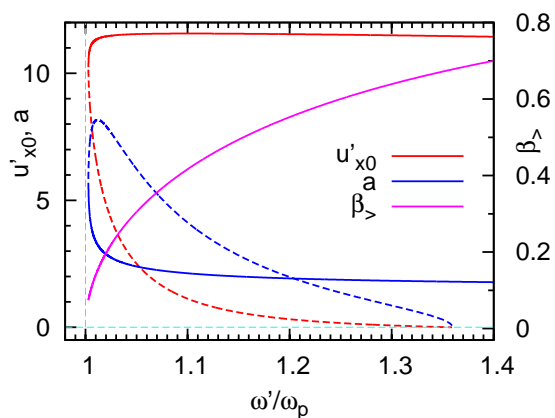


Fig. 1.— The circularly polarized modes that satisfy the jump conditions for  $\mu = 12$ ,  $\sigma = 3$  as a function of lab. frame frequency normalized to the proper plasma frequency. No solutions exist below a cut-off frequency that is close to  $\omega'/\omega_p = 1$ . Two solutions, one with  $u_{x0} \approx \mu$  and one with small  $u_{x0}$  (denoted by solid and dashed lines, respectively) exist above the cut-off, up to  $\omega'/\omega_p \approx 1.36$ , where  $a \rightarrow 0$  for the low- $u_{x0}$  mode. The modes have the same refractive index for given  $\omega'/\omega_p$ , which equals the speed  $\beta_{>}$  of the H-frame seen from the lab. frame.

a function of lab. frame frequency  $\omega'$  normalized to the (proper) plasma frequency  $\omega_p$ . In this example, we have chosen moderate values of the energy and momentum fluxes in the lab. frame:  $\mu = 12$ ,  $\sigma = 3$  (and, therefore,  $\Gamma_{<} = 3$ ), in order to display the structure of the solutions near the frequency cut-off. Since the wavenumber  $k$  vanishes in the H-frame, the refractive index is trivially obtained from the Lorentz transformation of the wave number and frequency:  $\omega' = \Gamma_{>}\omega$  and  $k' = \beta_{>}\Gamma_{>}\omega/c$ , (this also applies, of course, to the case of linear polarization) and the dispersion relation  $\omega = \omega_p$  implies  $\omega'/\omega_p = \Gamma_{>}$ . However, the corresponding strength parameter  $a$  is found only after solving the full set of equations. As can be seen from this figure, there are no physical solutions for  $\omega' < \omega_0$ , two solutions for  $\omega_0 < \omega' < \omega_1$  and only one physical solution for  $\omega' > \omega_1$ . (The full expressions for  $\omega_{0,1}$  are cumbersome, but for  $\mu \gtrsim \sigma^{3/2} \gg 1$  (corresponding to a mildly supermagnetosonic outflow), one finds  $\omega_0 \approx \omega_p [1 + (4\mu^2 - \sigma^3)\sigma / (32\mu^4) + O(\mu^{-5/3})]$  and  $\omega_1 \approx \omega_p (\mu/8)^{1/4} [1 + O(\mu^{-1/3})]$ , (cf. Kirk 2010).) Thus, the imposition of a finite energy flux per particle prohibits wave propagation at frequencies close to the cut-off  $\omega' = \omega_p$  found from linear theory. At intermediate frequencies, waves of two different amplitudes, and different values of  $u_{x0}$  are available to transport the required fluxes. One of these disappears ( $a \rightarrow 0$ ) at finite  $\omega'/\omega_p$ , leaving only a single solution of the jump conditions at high frequency.

In the case of a pulsar wind, the wave frequency is dictated by the rotation of the neutron star, but the plasma density decreases with increasing distance from the star. Thus, rather than solving the jump conditions as a function of frequency, more insight can be gained by solving as a function of radius. The connection between flux density and radius is found in terms of the luminosity per unit solid angle of the (radial) wind,  $dL/d\Omega_s$ :

$$\langle F' \rangle = \frac{1}{r^2} \frac{dL}{d\Omega_s}, \quad (27)$$

which can be expressed in dimensionless form in terms of the quantity

$$a_L = \sqrt{\frac{4\pi e^2}{m^2 c^5} \frac{dL}{d\Omega_s}}. \quad (28)$$

Physically,  $a_L$  is the strength parameter of the circularly polarized vacuum wave that would be needed to carry the entire pulsar luminosity at the surface  $\rho = 1$ . For a spherically symmetric wind  $a_L = 3.4 \times 10^{10} L_{38}^{1/2}$ , where  $L_{38} = L / (10^{38} \text{ erg s}^{-1})$ . This quantity is related to the *multiplicity* parameter  $\kappa$ , defined as the Goldreich-Julian charge density at the light cylinder divided by  $e$  (see, for example Lyubarsky & Kirk 2001; Kirk & Mochol 2011a) by

$$\kappa = a_L / (4\mu) \quad (29)$$

Writing the energy flux density as  $\mu \langle J' \rangle$  leads to the expression

$$\langle J' \rangle = \frac{2n_0 c \Gamma_{>}^2 \omega^2 a_L^2}{\rho^2 \omega_p^2 \mu}. \quad (30)$$

Applying this to the case of circular polarization, where  $\langle J' \rangle = 2n_0 u'_{x0}$  and  $\omega = \omega_p$ , one finds  $u'_{x0} = \Gamma_{>}^2 a_L^2 / (\mu \rho^2)$ . Then, the inequalities  $u'_{x0} < \gamma' \leq \mu$  and  $\Gamma_{>} > 1$  imply that circularly polarized waves propagate only when  $\rho > a_L / \mu$ . We therefore introduce the dimensionless scaled radius

$$\begin{aligned} R &= \rho \mu / a_L \\ &= \rho \kappa / 4 \end{aligned} \quad (31)$$

which can be constructed after solving the jump conditions from the expression

$$R = \frac{\Gamma_{>} \omega}{\omega_p} \sqrt{\frac{2\mu}{\gamma_0 (\langle J' \rangle / n_0 \gamma_0)}} \quad (32)$$

for both circularly and linearly polarized modes.

Figure 2 shows the properties of circularly polarized waves as functions of  $R$  for parameters appropriate to pulsar winds:  $\sigma = 100$  and  $\mu = 10100$  (and, therefore,  $\Gamma_{<} = 100$ ).

Near the cut-off radius, which lies close to  $R = 1$ , the mode properties are similar to those seen in Fig. 1, except that the refractive index, now plotted as a function of radius, is no longer degenerate. The detailed properties of these solutions have been discussed in Kirk (2010). However, note that these curves do not describe the radial evolution of a wave packet, as erroneously suggested in that paper and assumed by Asseo et al. (1984) (who considered linear polarization), but simply specify the wave modes into which a wind of given  $\mu$  and  $\sigma$  can convert at a given radius. The difference arises because the radial momentum flux density,  $\nu$ , is not a conserved quantity in the radial evolution of the superluminal modes (see also Kirk & Mochol 2011b).

### 3.2. Linear polarization

When the phase-averaged magnetic field vanishes, the properties of linearly polarized modes are similar to those of circularly polarized modes. This is illustrated in Fig. 3, where one sees that the refractive indices are practically identical.

This figure also shows the nonlinearity parameter  $q$ . For linear polarization,  $q$  is defined in terms of quantities measured at phase zero. This point in the wave is, however, special. It corresponds to the turning points of the “saw-tooth“ waveform (Max & Perkins 1971), where the fluid velocity either vanishes or lies precisely in the propagation direction. These points do not play a large role in determining the average properties of the wave. As a result,  $q$  varies substantially, especially close to points where  $u_{x0}$  changes sign ( $\log(R) \approx 0.4$  in the figure). One consequence is that an expansion of the fluxes using  $q$  as a small parameter is inadequate over most of the range relevant for pulsars, despite the fact that the waves are highly nonlinear (see the discussion in §4). In the case of circular polarization, the quantities that enter into the definition of  $q$  (Eq. 7) are phase-independent. The value of  $q$  is a useful characterization of the mode in this case, and Fig. 3 clearly illustrates that



one of the two solutions for given  $R$  is a relatively weak wave, with  $q \sim \text{few}$ , whereas the other is stronger, with  $q \sim 10^{-2}$ .

The properties of linearly polarized waves which carry a non-zero phase-averaged magnetic field in the toroidal direction are shown in Fig. 4. The refractive index is plotted for superluminal waves that correspond to  $\mu = 10100$ ,  $\sigma = 100$ , and four different values of the parameter  $b$ , that describes the relative amount of phase-averaged magnetic flux carried in the subluminal wave (see Eq. 25). It can be seen that the cutoff moves to greater  $R$  as  $b$  rises. In the striped wind model, this corresponds to moving away from the equator, where  $b = 0$ .

Although the refractive indices for non-zero  $b$  have similar shape to those for  $b = 0$ , there is one potentially important difference: for  $b > 0.65$  the lower branch cuts across the  $\beta_{\parallel} = 0$  axis, and continues towards solutions with negative phase speed. Zero refractive index indicates that the H-frame coincides with the lab. frame. These solutions are standing waves in the pulsar wind, with constant magnetic field and wavelength  $\gg r_{\text{LC}}$ . Negative refractive index indicates propagation towards the pulsar, in the sense that the velocity of the H-frame is inward propagating. Nevertheless these modes still carry the particle, energy, momentum and magnetic fluxes outwards towards the nebula.

Conversion of a subluminal wave into a superluminal wave is accompanied by a substantial transfer of energy from the fields to the particles. This is quantified in Fig. 5, where the phase-averaged Lorentz factor  $\langle \gamma' \rangle$  seen in the lab. frame is plotted as a function of  $R$ , for the same values of  $\mu$ ,  $\sigma$ , and  $b$  as in Fig. 4. For the smaller  $b$  values,  $b = 0$  and  $b = 0.2$ , the upper branch of the solution has  $\langle \gamma' \rangle \approx \mu$ , which implies that almost all of the field energy is converted to particles in the equatorial regions of the wind. At higher latitudes, only a part of the Poynting flux can be converted, since the phase-averaged magnetic flux cannot be dissipated. However, even at  $b = 0.95$ , the upper branch of the

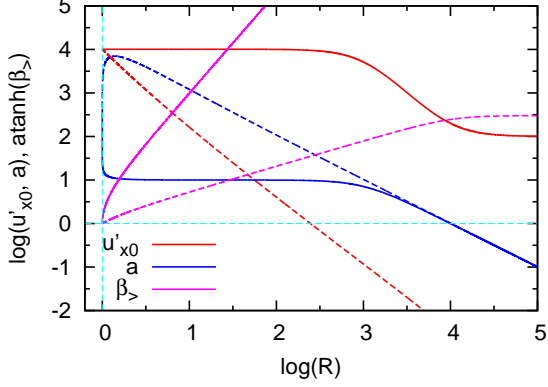


Fig. 2.— The properties of circularly polarized waves for  $\mu = 10100$ ,  $\sigma = 100$ , as a function of dimensionless radius in the pulsar wind. The inverse hyperbolic tangent of the refractive index  $ck'/\omega' = \beta_{>}$  is plotted, in order to bring out both the nonrelativistic regime,  $\beta_{>} \ll 1$ , near  $R = 1$  and the relativistic regime,  $\Gamma_{>} \gg 1$ , at  $R \gg 1$ .

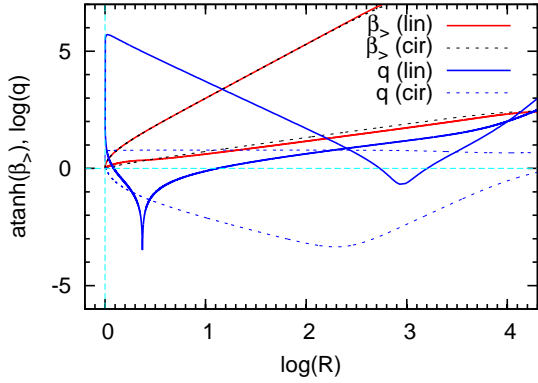


Fig. 3.— A comparison of the refractive indices for circularly and linearly polarized modes for  $\mu = 10100$ ,  $\sigma = 100$ . The nonlinearity parameter  $q$ , defined in (7), is also plotted for each mode.

dispersion relation carries particles with a mean Lorentz factor one order of magnitude larger than those of the incoming, striped wind solution.

### 3.3. Latitude dependence

According to the above figures, superluminal waves cannot propagate in the inner parts of a pulsar wind. The radius at which propagation becomes possible is close to  $R = 1$  for vanishing phase-averaged magnetic field, and rises with this quantity. However, in the striped wind model, the luminosity of the wind, and, hence, the parameter  $a_L$  is a function of latitude. In particular, the energy flux carried by the fields is proportional to  $\sin^2 \theta$ , where  $\theta$  is the colatitude, (measured from the rotation axis). The flux carried by the particles, on the other hand, is expected to be much smaller, but its angular dependence is uncertain. Assuming, for simplicity, that the ratio  $\sigma$  of these fluxes is independent of colatitude, one has

$$a_L = a_{L,\text{eq}} \sin \theta \quad (33)$$

$a_{L,\text{eq}} = 4.2 \times 10^{10} L_{38}^{1/2}$ , is the value of  $a_L$  in the equatorial plane.

The dependence of the average magnetic field carried by the striped wind on latitude depends on the inclination angle  $\alpha$  between the magnetic and rotation axes. Two current sheets are present in the striped wind, located at phases

$$\begin{aligned} \phi &= \pm \phi_{\text{sheet}} + 2n\pi \\ &= \pm \arccos(\cot \alpha \cot \theta) + 2n\pi \ , \end{aligned} \quad (34)$$

where  $n$  is an integer (Kirk et al. 2002). At  $\theta = \text{atan}(\cot \alpha)$ , the sheets merge, and vanish at higher latitudes (smaller colatitudes  $\theta$ ). At these sheets, the magnetic field reverses

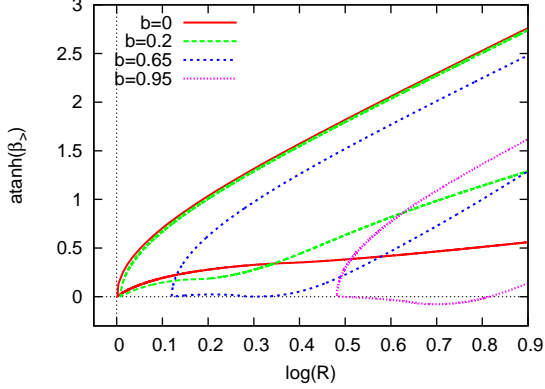


Fig. 4.— The inverse hyperbolic tangent of the refractive index  $\beta_{>}$  for linearly polarized waves that correspond to an incoming striped wind with  $\mu = 10100$ ,  $\sigma = 100$ , and four different values of the phase-averaged magnetic field  $b$ , as defined in Eq. (25)

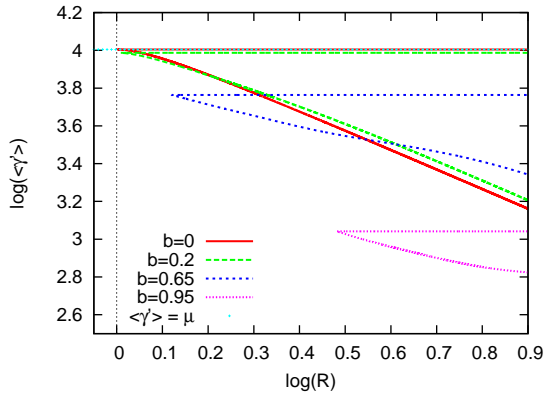


Fig. 5.— The mean Lorentz factor of the outflow particles  $\langle\gamma'\rangle$  measured in the lab. frame, for the linearly polarized superluminal wave solutions. Particles in a cold MHD outflow with the same energy and momentum flux have a Lorentz factor of 100 in this example ( $\mu = 10100$ ,  $\sigma = 100$ ). For the smaller  $b$  values,  $\langle\gamma'\rangle \sim \mu$ , implying a substantial fraction of the field energy has been transferred to the particles.

direction, so that

$$\begin{aligned} b(\theta, \alpha) &= \left( - \int_0^{\phi_{\text{sheet}}} d\phi + \int_{\phi_{\text{sheet}}}^{\pi} d\phi \right) / \pi \\ &= 1 - 2 \arccos(\cot \alpha \cot \theta) / \pi \end{aligned} \quad (35)$$

At those latitudes where there are no sheets, the striped wind model predicts an azimuthally symmetric magnetic field, i.e., no wave.

From curves similar to those plotted in Fig. 4 it is possible, for each value of  $b$ , to identify the critical radius inside which the mode cannot propagate. This can then be interpolated to give a function  $R_{\text{cr}}(b)$ . Together with the definition  $R_{\text{cr}} = \rho_{\text{cr}} \mu / a_{\text{L}}$ , this leads to

$$\frac{\mu \rho_{\text{cr}}}{a_{\text{L,eq}}} = \sin \theta R_{\text{cr}} [b(\theta, \alpha)] . \quad (36)$$

This surface is plotted in Fig. 6, for the case of the perpendicular rotator (magnetic inclination angle  $\alpha = \pi/2$ ), and, in Fig. 7, for various values of  $\alpha$ .

The location of the termination shock is determined by the balance between the momentum flux carried by the wind and the external pressure. If we make the reasonable assumption that the latter is independent of latitude, the approximate location  $\rho_{\text{ts}}(\theta)$  of the shock is given for  $\sigma \gg 1$  by (Lyubarsky 2002, Eq. 9):

$$\left( \frac{d\rho_{\text{ts}}}{d\theta} \right)^2 + \rho_{\text{ts}}^2 = \rho_0^2 \sin^2 \theta \quad (37)$$

where  $\rho_0$  is a constant. The normalization of the radius of the termination shock surface depends on the external pressure and has to be calculated for each individual object. In Fig. 6 three examples are shown, labeled by the ratio of the equatorial radius of the shock to that of the critical surface,  $\rho_{\text{eq,ts}}/\rho_{\text{eq,cr}}$ . It can be seen that if this ratio is significantly larger than unity, the cut-off surface falls almost entirely within the termination shock, except for a very small region close to the pole, where both surfaces have a cusp. A qualitatively

similar conclusion applies also for different magnetic inclination angles, as shown in Fig. 7: for  $\rho_{\text{eq,ts}}/\rho_{\text{eq,cr}} \gtrsim$  a few, almost the whole critical surface falls within the termination shock radius, apart from a small region at latitudes close to the magnetic inclination angle  $\alpha$ . The plots have been calculated using  $\mu = 10100$  and  $\sigma = 100$ , and show one quadrant of the poloidal plane. The 3D surface is generated by reflection in the  $\rho$  axis and rotation about the  $z$ -axis.

When the cut-off surface falls inside the termination shock, superluminal waves can propagate in the wind. It is therefore possible, if the ratio  $\rho_{\text{eq,ts}}/\rho_{\text{eq,cr}} > 1$ , that different modes coexist in the same wind but at different latitudes. The MHD description is more appropriate for the higher latitudes (close to  $\alpha$ ), and the superluminal wave solutions exist closer to the equatorial plane of the wind. If  $r_{\text{eq,ts}}/r_{\text{eq,cr}} < 1$ , no superluminal modes can be supported by the wind at any latitude. In the extreme case where  $r_{\text{eq,ts}}/r_{\text{eq,cr}} \gg 1$ , practically the whole wind can support these waves.

The above calculations have been conducted for  $\mu \approx 10^4$ . In this case the critical surface in the equatorial plane is located at  $\rho_{\text{cr}} \sim 10^7$  for the Crab pulsar, whereas the termination shock is located at roughly  $\rho_{\text{ts}} \sim 10^9$ . For the Vela pulsar, the critical radius lies at  $\rho_{\text{cr}} \sim 10^6$ , which is also well within the termination shock, located for this pulsar at  $\rho_{\text{ts}} \sim 10^8$  (Kargaltsev & Pavlov 2008). This value of  $\mu$ , corresponds to pair multiplicities of  $\kappa = 2.5 \times 10^6$  and  $\kappa = 2.5 \times 10^5$  for the Crab and Vela, respectively, much higher than conventional estimates (de Jager 2007), which would place the critical surface even closer to the pulsar. Thus, at least for young, energetic pulsars,  $\rho_{\text{eq,ts}}/\rho_{\text{eq,cr}} \gg 1$  and superluminal waves can propagate in essentially the entire equatorial wind.

However, the situation is different for pulsars which are members of binary systems, since the wind of the companion star can provide an obstacle capable of sustaining the termination shock relatively close to the pulsar. One example is the system PSR B1259-63,

containing a 48ms pulsar in an eccentric orbit about a B2e star. At periastron, the separation of the stars is  $\rho \sim 4.3 \times 10^4$ , while at apastron it becomes  $\rho \sim 6 \times 10^5$ . Very high-energy (TeV) gamma-rays were predicted to emerge from the termination shock of this pulsar (Kirk et al. 1999), and subsequently were detected (Aharonian et al. 2005, 2009; Abdo et al. 2011) at binary phases close to periastron. Assuming  $\mu \approx 10^4$  in this young pulsar, the critical radius at the equator is  $\rho_{\text{cr}} \sim 2.4 \times 10^5$ , which is greater than periastron but smaller than apastron separation. Therefore, if the termination shock created by the interaction of the stellar wind with the pulsar wind lies close to the B2e star, superluminal modes may play a role in determining its properties near apastron, but not near periastron. It would, therefore, be interesting to search for an observable diagnostic of this transition, such as an orbital modulation of the radiation from the shock front.

#### 4. Discussion

Nonlinear superluminal waves in electron-positron plasmas have been the subject of many papers over the last few decades. Nevertheless, their role in pulsar winds is still in need of clarification. One of the sources of this confusion is rooted in the use of the “strong wave limit” to simplify the treatment of linearly polarized waves (Max & Perkins 1971; Kennel et al. 1973; Kennel & Pellat 1976). This corresponds to taking only the lowest order terms in the parameter  $q$  defined in (7). To this order, the particle flux in the H-frame vanishes – particles are said to be “locked” into the wave in this frame. Furthermore, the energy densities of particles and fields are in equipartition to lowest order in  $q$ . These properties led Kennel et al. (1973) and Kennel & Pellat (1976) to assert that a strong wave would impose a rather severe upper limit on the particle flux from a pulsar.

The formulation we present in §2 and apply in §3 avoids this limit. It demonstrates that highly nonlinear superluminal waves can carry a substantial particle flux, although the

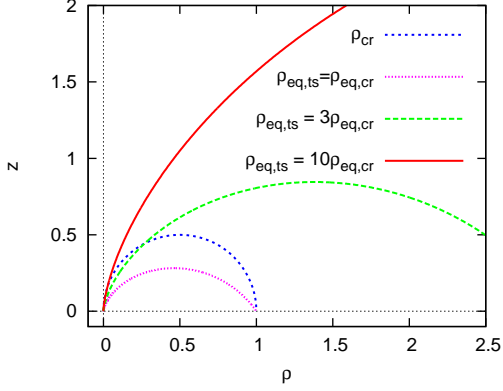


Fig. 6.— The surface  $\rho_{\text{cr}}$  outside of which superluminal waves propagate is shown for a perpendicular rotator ( $\alpha = \pi/2$ ). The pulsar is at the origin and  $z$  is the rotation axis. For comparison, the termination shock is also plotted for three different external pressures, such that its equatorial radius, normalized to that of  $\rho_{\text{cr}}$ , is 1, 3 and 10.

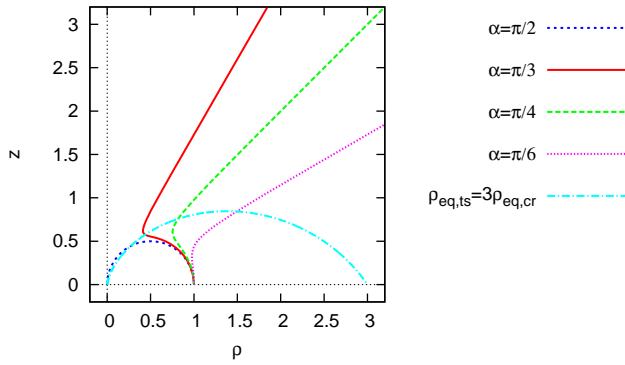


Fig. 7.— The critical surface  $\rho_{\text{cr}}$  for various inclination angles  $\alpha$  between the magnetic and rotation axes, superimposed on the termination shock surface whose equatorial radius is 3 times that of the critical surfaces.



minimum radius at which they can propagate moves outwards as the flux increases. These waves exhibit a wide range of  $q$  values (see Fig. 3). Particles are not locked into the wave motion in the H-frame, and energy is not necessarily in equipartition. Physically, the reason for this apparent contradiction is that  $q$  does not adequately characterize the wave solution, since it is defined at a highly non-representative point in the phase of the wave; there exists a large family of nonlinear waves that have no counterpart with  $q = 0$ .

The question of the stability of superluminal waves has attracted considerable attention. Asseo et al. (1978) found that radiation reaction would damp these waves within a few wavelengths, for parameters appropriate to the Crab pulsar. However, this conclusion was based on the  $q = 0$  limit discussed above, and may not apply to large  $q$  modes. Again working analytically in the limit  $q = 0$ , Asseo et al. (1980) found rapidly growing Weibel-like instabilities, but noted that they are stabilized when the phase-averaged magnetic field is sufficiently strong. For circular polarization, Lee & Lerche (1978, 1979) also found rapidly growing instabilities when the plasma is locked into the wave in the H-frame. Particle-in-cell simulations have been used by several authors to investigate this question. Leboeuf et al. (1982) injected a self-consistent wave and found it to be highly unstable when excited just above the cut-off frequency, but much less so when excited at higher frequencies. Skjæraasen et al. (2005) injected a nonlinear wave into a uniform plasma, and again found a strong instability that could be partially stabilized in the presence of streaming motion. Although our results do not address this question directly, it can be seen from the dispersion relations presented in Figs. 2 and 4 that the H-frame moves relativistically with respect to the pulsar ( $\Gamma_{>} \gg 1$ ) for  $R \gtrsim 10$ . An instability that grows locally in the H-frame with growth-rate comparable to the wave frequency in that frame, propagates a distance of  $\Gamma_{>}^2$  wavelengths in the pulsar reference frame in one  $e$ -folding time. Thus, although such instabilities may be present, their effect on the structure of the pulsar wind or the termination shock might not be dramatic.

In §3 we show that superluminal waves are capable of carrying the particle, energy and magnetic fields thought to be transported by a pulsar wind when they reach the termination shock of an isolated pulsar, except for a range of latitudes around the (rotation) pole. In fact, at most latitudes, there is a large range of radii between  $\rho_{\text{cr}}$  and  $\rho_{\text{ts}}$  in which propagation is possible. Our results do not address the question of where conversion from a striped wind to a superluminal wave might occur. However, since these waves are subsequently damped, it would seem likely that they could be sustained only within an extinction length of the termination shock itself, in which case their excitation and damping can be regarded as forming a part of this structure.

Lyubarsky (2003) suggested the physics of the “termination shock” should differ from that of an MHD shock and permit reconnection of the alternating component of the incoming magnetic field. A quantitative investigation based on analytic considerations and 1D PIC simulations (Pétri & Lyubarsky 2007) found that the effectiveness of reconnection depends on the ratio of the Larmor radii of electrons in the downstream flow to the wavelength of the stripes. Since this quantity increases monotonically with radius in a striped wind, these results imply that reconnection can be important only outside of a critical radius. Specifically, reconnection is predicted not to play a role for  $R < \pi/12$  (in our notation). At larger radii, the magnetic field is more effectively dissipated, until, at  $R > \pi\sqrt{\sigma}/3$ , full dissipation is achieved. However, this theory does not take account of the role of superluminal waves, although these waves are able to propagate in the region in which reconnection is predicted.

Sironi & Spitkovsky (2011), on the other hand, performed 2D and 3D PIC simulations. They found that the shock triggered reconnection, leading to full dissipation of the magnetic field, over the entire parameter range investigated. In our notation, this range extends over  $1/20 \lesssim R \lesssim 4$ . According to Fig. 4, superluminal waves of very high phase speed (small  $\beta_{\text{ph}}$ )

might be expected to play a role at the upper end of this range. However, the simulations do not appear to reveal their presence. The particle spectrum found in these simulations varies considerably, being closer to that observed in the Crab Nebula for lower values of  $R$ . However, as we show in §3, the termination shocks in the nebulae around isolated young pulsars are expected to lie much further from the pulsar than the range covered by these simulations, leaving us free to speculate that the physics controlling the structure and particle acceleration process might be substantially different in these objects.

## 5. Conclusions

We have reexamined the properties of transverse superluminal waves in an electron-positron plasma for parameters appropriate to pulsar winds. Our principal new results are:

- The properties of circularly and linearly polarized modes with vanishing phase-averaged magnetic field are similar (Fig. 3).
- The widely used strong-wave approximation ( $q = 0$ ), which underlies the assertion that these waves limit the particle flux, is inadequate. There is no wave-intrinsic limit on the particle flux.
- The cut-off surface, inside of which these waves cannot propagate, has a strong latitude dependence. (Fig. 7). It lies well inside the termination shock for young isolated pulsars, but must cross it at some phase of the binary orbit in the case of PSR B1259-63.
- At high latitudes, where the phase-averaged magnetic flux carried by the wind is large, long wavelength, quasi-homogeneous modes of infinite phase speed (i.e., with  $\beta \geq 0$ , Fig. 4) can arise close to the cut-off surface.

On the basis of these results, and of recent discussions in the literature of reconnection in the termination shock (Pétri & Lyubarsky 2007; Sironi & Spitkovsky 2011), we speculate that the physics of particle acceleration and the structure of this shock may be strongly influenced by the presence of superluminal waves.

### A. Two-fluid equations

Following Clemmow (1977) and Kennel & Pellat (1976), we present the solutions to the equations describing a cold, two-fluid plasma where *transverse* electromagnetic waves of superluminal phase speed can propagate. The equations are written in the H-frame and a plus (minus) index denotes positrons (electrons). It is convenient for the calculations to introduce complex quantities for the transverse four-velocity and the electric and magnetic fields:

$$u_{\perp,\pm} = u_{y,\pm} + iu_{z,\pm} \tag{A1}$$

$$E = E_y + iE_z \tag{A2}$$

$$B = B_y + iB_z \tag{A3}$$

Using these, the continuity equation and the equations of motion for each species, expressed in the H-frame, are:

$$\frac{d}{dt} (\gamma_{\pm} n_{\pm}) = 0 \tag{A4}$$

$$\gamma \frac{du_{\parallel,\pm}}{dt} = -\frac{e}{mc} \text{Im}(u_{\perp,\pm} B^*) \tag{A5}$$

$$\gamma \frac{du_{\perp,\pm}}{dt} = \frac{e}{mc} (\gamma E + iu_{\parallel,\pm} B) \tag{A6}$$

$$\gamma \frac{d\gamma_{\pm}}{dt} = \frac{e}{mc} \text{Re}(u_{\perp,\pm} E^*). \tag{A7}$$

where  $e$  is the magnitude of the electron charge.

In the H-frame, all space derivatives disappear. Conservation of magnetic flux,  $\nabla \cdot \mathbf{B} = 0$ , is automatic, and the remaining Maxwell's equations (Ampere, Faraday and Coulomb law, respectively) become:

$$\frac{1}{c} \frac{dE}{dt} = -4\pi e(n_+ u_{\perp,+} - n_- u_{\perp,-}) \quad (\text{A8})$$

$$\frac{dB}{dt} = 0 \quad (\text{A9})$$

$$4\pi\rho = 4\pi e(n_+ \gamma_+ - n_- \gamma_-) = 0. \quad (\text{A10})$$

where  $\rho$  is the charge density. From (A10), the charge density must vanish in the H-frame. In combination with the continuity equation, we get

$$n_+ \gamma_+ = n_0 \gamma_0 = n_- \gamma_- ,$$

where  $n_0, \gamma_0$  are constants. The restriction to purely transverse electric fields (which is implied in the way Ampere's law is expressed above) means that the radial current must vanish:  $n_+ u_{x+} = u_{x-} n_-$ . In this case, the net force acting on the plasma in the transverse direction vanishes, so that  $u_{y,z+} + u_{y,z-}$  is constant. In keeping with the approximation of toroidal fields (corresponding to the  $z$ -direction in the plane wave approximation) and radial propagation ( $x$ -direction), we set this constant to zero, so that  $u_{y+} = -u_{y-}$  and  $u_{z+} = -u_{z-}$ . Because of these relations, we can restrict ourselves to solving the equations for the positively charged fluid, and will henceforth drop the plus subscript for simplicity.

### A.1. Circular polarization

The simplest solution of these equations is the case of a circularly polarized wave.

Then  $B = 0$ , and we have:

$$u_{\perp} = u_{\perp 0} e^{i\omega_p t} \quad (\text{A11})$$

$$E = E_0 e^{i\omega_p t} \quad (\text{A12})$$

$$u_{\parallel} = u_0 \quad (\text{A13})$$

$$n = n_0 \quad (\text{A14})$$

The frequency coincides with the (proper) plasma frequency:

$$\omega_p = \sqrt{\frac{8\pi n_0 e^2}{m}} \quad (\text{A15})$$

and the magnitude of the perpendicular component of the four-momentum equals the *strength* or *nonlinearity* parameter  $a$ , defined using the electric field amplitude as

$$u_{\perp 0} = a \equiv \frac{e |E_0|}{mc\omega_p} \quad (\text{A16})$$

The parallel component of the four-velocity is a constant.

In the laboratory frame, which moves at speed  $-c/v_{\phi}$  as seen from the H-frame, the frequency of the wave is

$$\omega' = \Gamma_{>} \omega_{p0} \quad (\text{A17})$$

where  $\Gamma_{>}$  is the Lorentz factor of the transformation between the H-frame and the lab. frame.

### A.2. Linear polarization

Near the equatorial plane of a pulsar wind, the wave is linearly polarized and the relevant field components are the polar electric field and the toroidal magnetic field. In the

H-frame then, this requirement corresponds to  $E_z = 0$  and  $B_y = 0$ , i.e.,  $E = E_y$  becomes real and  $B = iB_z$  purely imaginary (and constant). It follows that the  $z$ -component of the four velocity is constant  $\text{Im}(u_\perp)$ . In a pulsar, a non-zero  $u_z$  corresponds to an azimuthal current loop, and, therefore, is proportional to the integrated magnetic flux crossing the enclosed surface. In the split-monopole geometry, this quantity falls off inversely with radius, and we set it to zero, so that  $u_\perp$  is a real variable.

Ampere's law becomes

$$\frac{dE}{d\phi} = -\frac{mc\omega}{e} \frac{u_\perp}{\alpha\gamma} \quad (\text{A18})$$

where  $\phi = \omega t$  and

$$\alpha = \frac{\omega^2}{\gamma_0\omega_p^2} . \quad (\text{A19})$$

Multiplying the equations of motion (A5) and (A6) by  $n$  and integrating, the four-velocity components can be expressed in terms of the variable  $y = E/E_0$ , the electric field normalized to the maximum value of its modulus (i.e.,  $-1 \leq y \leq 1$ ) as follows:

$$u_\parallel = u_0 + \alpha a^2 B_z (1 - y)/E_0 \quad (\text{A20})$$

$$\gamma = \gamma_0 + \frac{\alpha a^2}{2} (1 - y^2) \quad (\text{A21})$$

$$u_\perp^2 = \gamma^2 - u_\parallel^2 - 1 . \quad (\text{A22})$$

Having expressed all other unknowns in terms of the electric field, it remains to calculate the phase dependence of  $y$ , which is given by the equation

$$\alpha^2 a^2 \left( \frac{dy}{d\phi} \right)^2 = \frac{u_\perp^2}{\gamma^2} \quad (\text{A23})$$

or, explicitly:

$$\alpha^2 a^2 \left( \frac{dy}{d\phi} \right)^2 = \frac{N(y)}{[q/2 + (1 - y^2)]^2} \quad (\text{A24})$$

(Kennel & Pellat 1976) with  $q$ ,  $Q$  and  $b$  given by the expressions:

$$q = \frac{4\gamma_0}{\alpha a^2} \quad (\text{A25})$$

$$Q = 2 \left( 1 - \frac{u_0}{\gamma_0} \lambda \right) \quad (\text{A26})$$

$$\lambda = \frac{B_z}{E_0} . \quad (\text{A27})$$

and

$$N(y) = (1 - y)^2 [(y + 1)^2 - 4\lambda^2 - q] + (1 - y)qQ \quad (\text{A28})$$

is a quartic in  $y$ . Periodic waves exist if  $N$  has four real roots, which are (in order):

$$y_1 = \zeta \cos(\xi - 4\pi/3) - 1/3 \quad (\text{A29})$$

$$y_2 = \zeta \cos(\xi - 2\pi/3) - 1/3 \quad (\text{A30})$$

$$y_3 = 1 \quad (\text{A31})$$

$$y_4 = \zeta \cos(\xi) - 1/3 \quad (\text{A32})$$

where

$$\zeta = 2(4 + 12\lambda^2 + 3q)^{1/2} / 3 \quad (\text{A33})$$

$$\xi = \arccos \left[ \frac{3\sqrt{3}}{\sqrt{2}(\sqrt{3}u)^{3/2}} (16/27 + 2q/3 - 2\lambda q u_0 / \gamma_0 - 16\lambda^2/3) \right] \quad (\text{A34})$$

provided  $\xi$  is real.

The nonlinear dispersion relation follows by demanding that the change in phase in a half-cycle of the field oscillation equal  $\pi$ :

$$\pi = \int_{y_1}^1 \frac{dy}{dy/d\phi} \quad (\text{A35})$$

The phase-averaged value of a quantity  $A$  that depends on  $y$  is given by

$$\langle A \rangle = \frac{1}{\pi} \int_{y_1}^1 \frac{A(y)}{dy/d\phi} dy \quad (\text{A36})$$



If the phase-averaged magnetic field vanishes ( $\lambda = 0$ ),  $N(y)$  reduces to a quadratic in  $y^2$ , with  $y_2 = -1$  and  $y_3 = 1$ . In this case, the integrals in (A35) and (A36) can be expressed in closed form in terms of elliptic integrals, at least for the functions of interest. For non-zero  $\lambda$ , on the other hand,  $y$  oscillates between  $y_2 > -1$  and  $y_3 = 1$ . The dispersion relation and the phase-averages must then be evaluated by numerical integration.

The components of the stress energy tensor consists of a fluid and a field contribution. In the H-frame these are:

$$T_{\text{part}}^{00} = 2mc^2 \langle n\gamma^2 \rangle = 2n_0\gamma_0 mc^2 \langle \gamma \rangle \quad (\text{A37})$$

$$T_{\text{part}}^{01} = 2mc^2 \langle n\gamma u_x \rangle = 2n_0\gamma_0 mc^2 \langle u_x \rangle \quad (\text{A38})$$

$$T_{\text{part}}^{11} = 2mc^3 \langle nu_x^2 \rangle = 2n_0\gamma_0 mc^3 \left\langle \frac{u_x^2}{\gamma} \right\rangle \quad (\text{A39})$$

for the fluids, and

$$T_{\text{EM}}^{00} = \frac{\langle E^2 \rangle + B^2}{8\pi} = \frac{\langle y^2 \rangle + \lambda^2}{8\pi} E_0^2 \quad (\text{A40})$$

$$T_{\text{EM}}^{01} = \frac{c\langle E \rangle B}{4\pi} = \frac{c\langle y \rangle \lambda E_0^2}{4\pi} \quad (\text{A41})$$

$$T_{\text{EM}}^{11} = T_{\text{EM}}^{00} \quad (\text{A42})$$

for the fields. For the circularly polarized modes,  $\lambda = 0$ ,  $\langle y \rangle = 0$ , and  $\langle y^2 \rangle = 1$ . In addition,  $u_x = u_{x0}$  and  $\gamma = \gamma_0$  are phase-independent.

## B. Lorentz boosts

The phase-averaged particle flux, energy, energy flux, and  $x$ -momentum flux densities and the electric field transform according to:

$$J' = \Gamma_{>} (2\beta_{>} n_0 \gamma_0 + J) \quad (\text{B1})$$

$$T'^{00} = \Gamma_{>}^2 (T^{00} + \beta_{>} T^{01} + \beta_{>}^2 T^{11}) \quad (\text{B2})$$

$$T'^{01} = \Gamma_{>}^2 [(1 + \beta_{>}^2) T^{11} + \beta_{>} (T^{00} + T^{11})] \quad (\text{B3})$$

$$T'^{11} = \Gamma_{>}^2 (T^{11} + 2\beta_{>} T^{01} + \beta_{>}^2 T^{00}) \quad (\text{B4})$$

$$\langle E' \rangle = \Gamma_{>} (\beta_{>} \lambda E_0 + \langle E \rangle) \quad (\text{B5})$$

## REFERENCES

- Abdo, A. A. et al. 2011, *ApJ*, 736, L11+, 1103.4108
- Aharonian, F. et al. 2009, *A&A*, 507, 389
- . 2005, *A&A*, 442, 1, arXiv:astro-ph/0506280
- Akhiezer, A., & Polovin, R. 1956, *Sov. Phys. JETP*, 3, 696
- Arons, J. 2011, in *High-Energy Emission from Pulsars and their Systems*, ed. D. F. Torres & N. Rea, 165–+, 1009.2798
- Asseo, E., Kennel, C. F., & Pellat, R. 1978, *A&A*, 65, 401
- Asseo, E., Kennel, F. C., & Pellat, R. 1975, *A&A*, 44, 31
- Asseo, E., Llobet, X., & Pellat, R. 1984, *A&A*, 139, 417
- Asseo, E., Llobet, X., & Schmidt, G. 1980, *Phys. Rev. A*, 22, 1293
- Begelman, M. C. 1998, *ApJ*, 493, 291, arXiv:astro-ph/9708142
- Clemmow, P. C. 1974, *Journal of Plasma Physics*, 12, 297
- . 1977, *Journal of Plasma Physics*, 17, 301
- Coroniti, F. V. 1990, *ApJ*, 349, 538
- de Jager, O. C. 2007, *ApJ*, 658, 1177
- Gaensler, B. M., & Slane, P. O. 2006, *Ann. Rev. Astron. Astrophys*, 44, 17, arXiv:astro-ph/0601081
- Iwamoto, N. 1993, *Phys. Rev. E*, 47, 604

- Kargaltsev, O., & Pavlov, G. G. 2008, in American Institute of Physics Conference Series, Vol. 983, 40 Years of Pulsars: Millisecond Pulsars, Magnetars and More, ed. C. Bassa, Z. Wang, A. Cumming, & V. M. Kaspi, 171–185, 0801.2602
- Kaw, P., & Dawson, J. 1970, *Physics of Fluids*, 13, 472
- Kennel, C. F., & Pellat, R. 1976, *Journal of Plasma Physics*, 15, 335
- Kennel, C. F., Schmidt, G., & Wilcox, T. 1973, *Physical Review Letters*, 31, 1364
- Kirk, J. G. 2010, *Plasma Physics and Controlled Fusion*, 52, 124029, 1008.0536
- Kirk, J. G., Ball, L., & Skjaeraasen, O. 1999, *Astroparticle Physics*, 10, 31, arXiv:astro-ph/9808112
- Kirk, J. G., Lyubarsky, Y., & Petri, J. 2009, in *Astrophysics and Space Science Library*, Vol. 357, *Astrophysics and Space Science Library*, ed. W. Becker, 421–+
- Kirk, J. G., & Mochol, I. 2011a, *ApJ*, 729, 104, 1012.0307
- . 2011b, *ApJ*, 736, 165
- Kirk, J. G., & Skjæraasen, O. 2003, *ApJ*, 591, 366, arXiv:astro-ph/0303194
- Kirk, J. G., Skjæraasen, O., & Gallant, Y. A. 2002, *A&A*, 388, L29, arXiv:astro-ph/0204302
- Leboeuf, J. N., Ashour-Abdalla, M., Tajima, T., Kennel, C. F., Coroniti, F. V., & Dawson, J. M. 1982, *Phys. Rev. A*, 25, 1023
- Lee, M. A., & Lerche, I. 1978, *Journal of Plasma Physics*, 20, 313
- . 1979, *Journal of Plasma Physics*, 21, 43
- Lyubarsky, Y. 2010, *ApJ*, 725, L234, 1012.1411

- Lyubarsky, Y., & Kirk, J. G. 2001, *ApJ*, 547, 437, arXiv:astro-ph/0009270
- Lyubarsky, Y., & Liverts, M. 2008, *ApJ*, 682, 1436, 0805.0085
- Lyubarsky, Y. E. 2002, *MNRAS*, 329, L34
- . 2003, *MNRAS*, 345, 153, arXiv:astro-ph/0306435
- Max, C., & Perkins, F. 1971, *Physical Review Letters*, 27, 1342
- Melatos, A., & Melrose, D. B. 1996, *MNRAS*, 279, 1168
- Michel, F. C. 1969, *ApJ*, 158, 727
- . 1994, *ApJ*, 431, 397
- Pétri, J. 2011, *MNRAS*, 412, 1870, 1011.3431
- Pétri, J., & Dubus, G. 2011, *MNRAS*, 1193, 1104.4219
- Pétri, J., & Kirk, J. G. 2005, *ApJ*, 627, L37, arXiv:astro-ph/0505427
- Pétri, J., & Lyubarsky, Y. 2007, *A&A*, 473, 683
- Rees, M. J., & Gunn, J. E. 1974, *MNRAS*, 167, 1
- Sironi, L., & Spitkovsky, A. 2011, *ArXiv e-prints*, 1107.0977
- Skjæraasen, O., Melatos, A., & Spitkovsky, A. 2005, *ApJ*, 634, 542, arXiv:astro-ph/0508192
- Spitkovsky, A. 2006, *ApJ*, 648, L51, arXiv:astro-ph/0603147
- Usov, V. V. 1975, *Ap&SS*, 32, 375